Optics Letters

Laser-based optoelectronic generation of narrowband microwave chaos for radars and radio-communication scrambling

YANNE K. CHEMBO[1,2]

[1]FEMTO-ST Institute, Univ. Bourgogne Franche-Comté, CNRS, Optics Department, 15B Avenue des Montboucons, 25030 Besançon Cedex, France
[2]GeorgiaTech-CNRS Joint International Laboratory [UMI 2958], Atlanta Mirror Site, School of Electrical and Computer Engineering, 777 Atlantic Dr. NW, Atlanta, Georgia 30332, USA (yanne.chembo@femto-st.fr)

Received 20 June 2017; revised 3 August 2017; accepted 4 August 2017; posted 4 August 2017 (Doc. ID 299367); published 28 August 2017

This Letter proposes an optoelectronic oscillator architecture for narrowband microwave chaos generation. In the time domain, the microwave signal features a slowly varying envelope with amplitude and phase chaos while, in the frequency domain, it is quasi-indistinguishable from a band-limited white noise. A full theoretical analysis is performed to investigate the stability properties and route to chaos for the microwave oscillations. We experimentally generate the narrowband microwave chaos with a central frequency of 3 GHz and a bandwidth of only 16 MHz, and we discuss the applications for radar engineering and radio-communication scrambling.

OCIS codes: (060.2310) Fiber optics; (060.5625) Radio frequency photonics; (230.0250) Optoelectronics; (230.4910) Oscillators; (350.4010) Microwaves.

https://doi.org/10.1364/OL.42.003431

The persistent trend of using chaotic signals for technological purposes has been significantly consolidated in recent years. The first application has been chaos cryptography, where a chaotic carrier is used to mask an information bearing signal, which is later decrypted using the chaos-pass filtering properties of synchronization [1–4]. If such an encryption scheme has been thoroughly investigated within the frame of optical fiber communication networks, the issue of applying the same method to radio-frequency (RF) networks becomes a pertinent topic (see Refs. [5,6]). On the one hand, these networks are extremely vulnerable to eavesdropper attacks, as they are essentially open-space networks, where virtually anyone has access to the carrier; hence, microwave chaos cryptography may enable safe communication safely in these kinds of open-access networks. On the other hand, chaotic carriers may be used to scramble the RF traffic in a limited frequency band and in a limited area, while giving at the same time to an authorized receiver the possibility to still have a transparent network through a synchronization-based unscrambling scheme. In both cases, the microwave carrier should ideally have a central frequency laying ultra-high (UHF) and super-high (SHF) frequency bands (ranging from 0.3 to 30 GHz), and a relatively narrow bandwidth (few tens of megahertz, upper limit) in order to respect spectrum management requirements impeding the use of broadband microwave signals in open-space, shared networks. Narrowband chaos can also be useful in optical communications, as it can serve to encrypt only one or a few channels in a wavelength-division multiplexed optical carrier containing many more channels that do not need to be encrypted.

Chaotic microwaves have also recently emerged as interesting probe references in random signal radars [7–12]. In this case, the emitting antenna sends a chaotic microwave with an echo that is unambiguously recognizable from any other through the unique spectral and temporal signature of deterministic chaos. Along the same line, time slots of a chaotic time series are orthogonal (that is, uncorrelated if separated by a time-lag greater than the inverse of the smallest Lyapunov exponent) so that they do not interfere and, thereby, allow for multi-user, multi-task architectures.

In this Letter, we propose a versatile microwave chaos generator, potentially able to provide a microwave signal of any central frequency in the UHF and SHF bands, with a bandwidth that can be set to virtually any value. Our aim is to provide a system able to fulfill the aforementioned requirements for radar and scrambling applications, as well as for other microwave photonics applications.

Our experimental system belongs to the family of optoelectronic oscillators [3,13]. A schematic representation of the system under study is displayed in Fig. 1, and it consists of the following elements: (*1*) a continuous-wave semiconductor laser of power P and wavelength $\lambda = 1550$ nm; (*2*) a wideband integrated optics $LiNbO_3$ Mach–Zehnder (MZ) modulator, seeded by the laser (this modulator is characterized by its half-wave voltages $V_{\pi_{DC}} = 5.3$ V and $V_{\pi_{RF}} = 4.2$ V; (*3*) a few-meter- long fiber delay line; (*4*) a fast amplified photodiode with a conversion factor S; (*5*) a narrowband microwave RF filter of central frequency $F_0 = \Omega_0/2\pi = 3$ GHz and −3 dB bandwidth $\Delta F = \Delta\Omega/2\pi = 16$ MHz, intended to

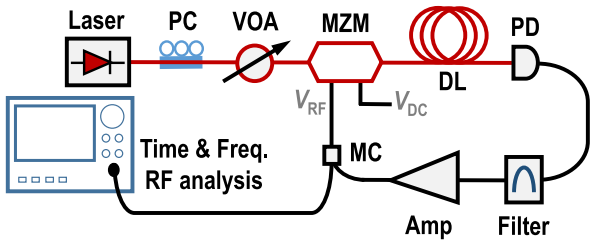

Fig. 1. Experimental setup for the narrowband microwave chaos generator optoelectronic oscillator. PC, polarization controller; VOA, variable optical attenuator; MZM, Mach–Zehnder modulator; DL, delay line; PD, photodiode; Filter, narrowband bandpass filter; Amp, RF amplification; MC, microwave coupler.

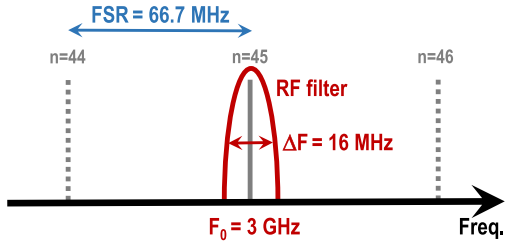

Fig. 2. Modal structure of the microwave generator. The ring cavity modes induced by the time delay are spaced by a free spectral range, FSR $\simeq$ 66.7 MHz, which is larger than the bandwidth $\Delta F =$ 16 MHz of the narrowband filter. Therefore, *only one* mode can oscillate, and the chaotic dynamics are not induced by multimode interactions.

select the frequency range of interest for the chaotic microwave signal; and (6) microwave amplifiers to close the loop back to the modulator. In order to obtain sufficiently high gain values, we have cascaded two RF amplifiers, which are driven close to saturation and, therefore, operate nonlinearly. The whole optoelectronic delay line yields an overall delay time $T = 15$ ns. All optical and electrical losses are gathered in a single attenuation factor κ. The data acquisition and processing involve numerical filtering to isolate the microwave frequency of interest.

This kind of narrowband optoelectronic oscillator has been extensively studied in the context of ultra-stable microwave generation [14–20]. It should also be noted that this architecture is characterized by a very high degree of synchronizability [21–24], a feature that is particularly important for our targeted applications. The variable of interest here is the microwave voltage signal $V(t)$ at the input of the MZ modulator. It has yet been demonstrated that its dimensionless counterpart $x(t) = \pi V(t)/2V_{\pi_{\mathrm{RF}}}$ obeys an Ikeda-like equation (see Ref. [25–27]) that has the particularity to feature an integro-differential term [28–31], following

$$x + \tau\frac{dx}{dt} + \frac{1}{\theta}\int_{t_0}^{t} x(\xi)\mathrm{d}\xi = \beta\cos^2[x(t-T)+\phi], \quad (1)$$

with $\tau = 1/\Delta\Omega$ and $\theta = \Delta\Omega/\Omega_0^2$. The parameter $\beta = \pi\kappa SGP/2V_{\pi_{\mathrm{RF}}}$ is the normalized feedback gain (G being the amplifier gain in the linear approximation), while $\phi = \pi V_B/2V_{\pi_{\mathrm{DC}}}$ is the MZ offset phase. The dynamics of this equation critically depend on the values of its various parameters [32–35]. In the present case, owing to the narrowband nature of the filter, we can represent the solution $x(t)$ under the form of a carrier of frequency Ω_0, slowly modulated by a complex amplitude $\mathcal{A}(t)$, following [31]

$$x(t) = \frac{1}{2}\mathcal{A}(t)e^{i\Omega_0 t} + \frac{1}{2}\mathcal{A}^*(t)e^{-i\Omega_0 t}, \quad (2)$$

with $\mathcal{A} = Ae^{i\psi}$. Therefore, the slowly varying amplitude obeys the equation [31]

$$\frac{d\mathcal{A}}{dt} = -\mu e^{i\vartheta}\mathcal{A} - 2\gamma\mu e^{i\vartheta}\mathrm{Jc}_1[2|\mathcal{A}_T|]e^{-i\sigma}\mathcal{A}_T, \quad (3)$$

where we have adopted the notation $\mathcal{A}_T \equiv \mathcal{A}(t-T)$. The above equation allows the study of the deterministic dynamics of the system, with all stochastic effects being overlooked. The parameters of this equation are the round-trip phase shift of the microwave signal $\sigma = \Omega_0 T$, and the effective gain of the feedback loop $\gamma = \beta\sin 2\phi$. The Bessel-cardinal function Jc_1, defined as $Jc_1(x) = J_1(x)/x$, with $\mathrm{Jc}_1(0) = \frac{1}{2}$ by continuity is the nonlinear transfer function of the feedback loop for the microwave signal. The filter parameters are $\mu = [\Delta\Omega/2]\{1 + [1/(2Q)]^2\}^{-1/2}$ and $\vartheta = \arctan[1/2Q]$, with $Q = \Omega_0/\Delta\Omega \sim 200$ being the quality factor of the RF filter. Since the Q-factor of the filter is generally high, we may simply consider that $\mu \simeq \Delta\Omega/2$ and $\vartheta \simeq 1/(2Q) \to 0$ in the most simple approximation [31,36]. It is important to note that the free spectral range (FSR) of the oscillating loop is equal to FSR $= 1/T = 66.67$ MHz, which is significantly larger than its RF bandwidth $\Delta F = 16$ MHz. Therefore, there can be *only one* oscillating mode, which is precisely the ring cavity mode whose order n is the closest integer to the ratio F_0/FSR (here equal to 45; see Fig. 2).

The microwave envelope variable is complex and, therefore, enables the simultaneous study of the amplitude and the phase dynamics. The complexity of this dynamics principally depends on the value of the gain γ, which corresponds to the ratio between the input power (laser power, gain amplification) and the various power losses. It can be straightforwardly demonstrated that the trivial fixed point $\mathcal{A}_0 \equiv 0$ is stable when $|\gamma| < 1$, that is, when the input power is still inferior to the overall power losses in the feedback loop [31]. However, when $|\gamma| > 1$, the system starts to oscillate. As the system crosses the oscillation threshold $\gamma_{\mathrm{th}} = 1$, the system undergoes a bifurcation from the trivial fixed point to the stationary solution $\mathcal{A}_0 = A_0 e^{i(\omega_0 t + \psi_0)}$, where ω_0 is a fixed detuning frequency from the central frequency Ω_0 of the RF filter, and ψ_0 is a constant phase that can be set to any arbitrary value.

From Eq. (3), it can be deduced that the detuning frequency obeys the nonlinear algebraic equation

$$\omega_0 = -\mu\sin\vartheta + \mu\cos\vartheta\tan[\vartheta - \sigma - \omega_0 T], \quad (4)$$

while the amplitude reads

$$A_0 = \frac{1}{2}\mathrm{Jc}_1^{-1}\left[-\frac{1}{2\gamma}\frac{\cos\vartheta}{\cos(\vartheta - \sigma - \omega_0 T)}\right], \quad (5)$$

where Jc_1^{-1} is the inverse Bessel-cardinal function, which only exists for $\gamma \geq 1$, and is single-valued for realistic gain values.

The stability of this stationary solution can be investigated using the standard techniques used for of delay-differential systems [37,38], based on the eigenvalue analysis of linearized perturbations. The asymptotic behavior of the amplitude and

phase perturbation variables δA and $\delta\psi$ are governed by the following flow:

$$\frac{d}{dt}\begin{bmatrix}\delta A\\ \delta\psi\end{bmatrix} = -\mu\cos\vartheta[\mathbf{J}]\begin{bmatrix}\delta A\\ \delta\psi\end{bmatrix} - \gamma\mu[\mathbf{K}]\begin{bmatrix}\delta A_T\\ \delta\psi_T\end{bmatrix}, \tag{6}$$

with

$$[\mathbf{J}] = \begin{bmatrix}1 & -A_0\tan\varphi\\ \frac{1}{A_0}\tan\varphi & 1\end{bmatrix}, \tag{7}$$

$$[\mathbf{K}] = \begin{bmatrix}2J_1'[2A_0]\cos\varphi & -J_1[2A_0]\sin\varphi\\ \frac{2}{A_0}J_1'[2A_0]\sin\varphi & \frac{1}{A_0}J_1[2A_0]\cos\varphi\end{bmatrix}, \tag{8}$$

where $\varphi = \vartheta - \sigma - \omega_0 T$. It appears that the perturbation for the amplitude and the phase are generally coupled. For the sake of exemplification, we are going to consider the particular case when the matrices $[\mathbf{J}]$ and $[\mathbf{K}]$ are almost diagonal, leading to uncoupled perturbations; this corresponds to the case $\sigma = \pi$ mod$[2\pi]$ and $\omega_0 T \sim \vartheta \sim 0$ mod$[2\pi]$, yielding $\sin\varphi \simeq \tan\varphi \simeq 0$. In that limit case, the phase is neutrally stable, while the real and imaginary parts λ_a and ω_a of the eigenvalue associated to the perturbation $\delta A = \delta A_0 e^{(\lambda_a + i\omega_a)t}$ obey the equations

$$\lambda_a = -\mu + 2\mu\gamma J_1'[2A_0]e^{-\lambda_a T}\cos\omega_a T, \tag{9}$$

$$\omega_a = -2\mu\gamma J_1'[2A_0]e^{-\lambda_a T}\sin\omega_a T. \tag{10}$$

The parameter $\alpha = 2\gamma J_1'[2A_{\mathrm{osc}}]$ rules the dynamical behavior close to the Hopf bifurcation of frequency ω_a that occurs exactly when $\lambda_a = 0$, that is, when $\alpha\cos\omega_a T = 1$. It can be shown that the bifurcation has an eigenfrequency

$$\omega_a = \frac{1}{T}\tan^{-1}\left[-\frac{1}{\mu T}\right], \tag{11}$$

with $\tan^{-1}$ being the inverse of the tangent cardinal function restricted to its domain of definition. Numerically, it is found that $\omega_a \simeq 0.31\times 2\pi/T$. On the other hand, using Eq. (5) and the equality $J_1'(x) = J_0(x) - \mathrm{Jc}_1(x)$, it can be deduced that the corresponding critical value γ_{cr} obeys the nonlinear algebraic equation

$$Jc_1^{-1}\left[\frac{1}{2\gamma_{\mathrm{cr}}}\right] = J_0^{-1}\left[\frac{1}{2\gamma_{\mathrm{cr}}}\left(1+\frac{1}{\cos\omega_a T}\right)\right], \tag{12}$$

where J_0^{-1} is the inverse of the Bessel function J_0 in the single-valued range. The real part of the eigenvalue is such that $\lambda_a < 0$ for $|\gamma| < \gamma_{\mathrm{cr}}$, and $\lambda_a > 0$ for $|\gamma| > \gamma_{\mathrm{cr}}$, so that the single-mode oscillation is stable below the critical value and unstable above: solving this equation yields the critical value $\gamma_{\mathrm{cr}} \simeq 4.0$.

This bifurcation behavior is presented in the diagram displayed in Fig. 3, which is obtained through the numerical simulation of Eq. (3). It can be seen that after the oscillation threshold at $\gamma = 1$, the amplitude grows and bifurcates around $\gamma \simeq 4.0$, as predicted analytically. Further increase of the gain leads to multi-periodic oscillations, and later to fully developed chaos. One should note that chaos arises here for significantly high values of the normalized gain ($|\gamma| \sim 8$), and it is induced by the modulator nonlinearity (regardless of the eventual saturation of the RF amplification). In comparison, chaos is obtained for $|\gamma| \sim 3$ in the usual configurations of optoelectronic oscillators featuring narrowband (~10 MHz) with long delay (~20 μs), or broadband (~10 GHz) with short delay

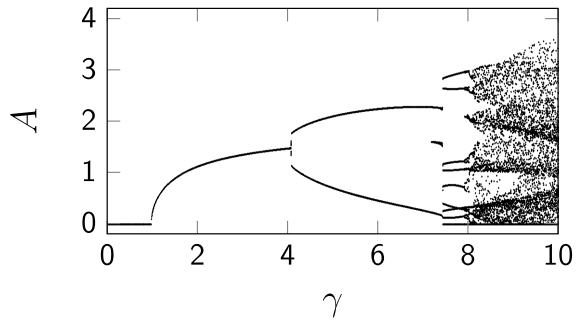

Fig. 3. Bifurcation diagram for the normalized amplitude A of the microwave signal as a function of the gain γ.

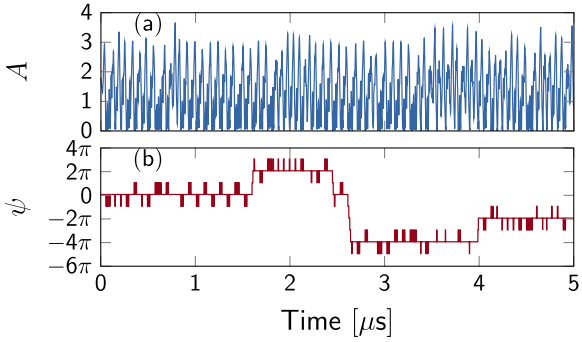

Fig. 4. Numerical simulation of Eq. (3) when the effective gain is set to $\gamma = 10$. (a) Amplitude dynamics. (b) Phase dynamics.

(~20 ns) (see, for example, review article [3]). The time-domain chaotic dynamics of the microwave signal envelope is displayed in Fig. 4. One can note that the amplitude of the signal is chaotically modulated in a timescale of a few tenths of microseconds, in accordance with the bandwidth of 16 MHz, and with a quite large modulation index (~1). The phase undergoes random phase jumps of $\pm\pi$, thereby indicating that the microwave signal remains highly coherent, and that the effect of chaos is mostly an amplitude modulation with phase-flip modulation.

An experimental chaotic time trace of the microwave signal variable $V(t)$ is presented in Fig. 5. As predicted theoretically,

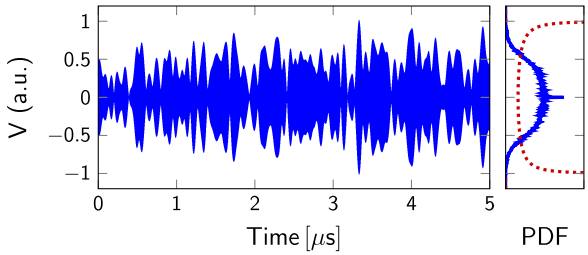

Fig. 5. Experimental time trace of the chaotically modulated microwave signal $V(t)$ of frequency ~3 GHz when the laser power is set at 0.2 mW, and V_B is biased such that $\phi \simeq \pi/4$. This microwave signal has been normalized such that its maximal value is equal to 1. The right panel displays the PDF of the chaotic microwave signal (continuous blue), which can be compared with that of a pure sinusoidal microwave signal with the same maximal amplitude (dotted red; note that this PDF is discontinuous at $V = \pm 1$, where it theoretically diverges).

reaching the chaotic regime requires very high gain ($\gamma > 8$; see Fig. 3), and this is why two cascaded RF amplifiers have been used in the electronic branch of the oscillator. The large chaotic amplitude modulation leads to a bell-shaped probability density function (PDF), which significantly differs from the convex and discontinuous PDF of the normalized sine wave of amplitude 1, which is $f(x) = [\pi\sqrt{1-x^2}]^{-1}$. Indeed, in a pure sine wave, the PDF diverges at the extrema: however, in our chaotically modulated microwave signal, the waveform remains quasi-sinusoidal on a fast scale ($\sim 1/F_0$), but extrema are pseudo randomly distributed in the slow scale ($\sim 1/\Delta F$). Therefore, the change of convexity induced by the chaotic modulation indicates that the full signal (and not just its envelope) features high entropy, despite its narrow bandwidth.

In conclusion, we have demonstrated a simple optoelectronic system that is able to generate narrowband microwave chaotic signals, that is, a microwave signal whose envelope is chaotic, while its fast-scale dynamics remains periodic. Our theoretical analysis consisted of a detailed analytical study, confirmed by numerical simulations. Experimental evidence of this microwave envelope chaos has also been provided. The flexibility of this system allows, in principle, the generation of these microwave signals around any frequency for which optoelectronic components are available (up to a few tens of gigahertz today). We anticipate that these kinds of signals should find applications in microwave chaos communications, as well as in the emergent field of broadband radar systems. Further investigations are in progress along these lines. Future research will also focus on deepening our understanding of the synchronization of such systems [22–24,39–41] and the exploration of the system's behavior when seeded with nonclassical light [42].

Funding. H2020 European Research Council (ERC) (278616, 632108); Centre National d'Etudes Spatiales (CNES), SHYRO; Labex ACTION; Region de Franche-Comte, CORPS.

Acknowledgment. The author would like to acknowledge fruitful discussions with Laurent Larger.

REFERENCES

1. A. Argyris, D. Syvridis, L. Larger, V. Annovazzi-Lodi, P. Colet, I. Fischer, J. Garcia-Ojalvo, C. R. Mirasso, L. Pesquera, and K. A. Shore, Nature **438**, 343 (2005).
2. R. Lavrov, M. Jacquot, and L. Larger, IEEE J. Quantum Electron. **46**, 1430 (2010).
3. L. Larger, Philos. Trans. R. Soc. A **371**, 20120464 (2013).
4. M. C. Soriano, J. Garcia-Ojalvo, C. R. Mirasso, and I. Fischer, Rev. Mod. Phys. **85**, 421 (2013).
5. L. Larger, V. S. Udaltsov, J.-P. Goedgebuer, and W. T. Rhodes, Electron. Lett. **37**, 594 (2001).
6. A. Pallavisini, L. Larger, V. S. Udaltsov, J.-M. Merolla, R. Quere, N. Butterlin, and J.-P. Goedgebuer, IEEE J. Quantum Electron. **43**, 426 (2007).
7. L. Illing and D. J. Gauthier, Chaos **16**, 033119 (2006).
8. S. Qiao, Z. G. Shi, K. S. Chen, W. Z. Cui, W. Ma, T. Jiang, and L. X. Ran, Prog. Electromagn. Res. **75**, 225 (2007).
9. M. S. Willsey, K. M. Cuomo, and A. V. Oppenheim, IEEE Trans. Aerosp. Electron. Syst. **47**, 1974 (2011).
10. M. Zhang, Y. Ji, Y. Zhang, Y. Wu, H. Xu, and W. Xu, IEEE Photon. J. **6**, 7902412 (2014).
11. J. Zheng, H. Wang, J. Fu, L. Wei, S. Pan, L. Wang, J. Liu, and N. Zhu, Opt. Express **22**, 4896 (2014).
12. T. Yao, D. Zhu, D. Ben, and S. Pan, Opt. Lett. **40**, 1631 (2015).
13. X. Zou, X. Liu, W. Li, P. Li, W. Pan, L. Yan, and L. Shao, IEEE J. Quantum Electron. **52**, 0601116 (2016).
14. X. S. Yao and L. Maleki, Electron. Lett. **30**, 1525 (1994).
15. X. S. Yao and L. Maleki, J. Opt. Soc. Am. B **13**, 1725 (1996).
16. J. Yang, Y. Jin-Long, W. Yao-Tian, Z. Li-Tai, and Y. En-Ze, IEEE Photon. Technol. Lett. **19**, 807 (2007).
17. R. M. Nguimdo, Y. K. Chembo, P. Colet, and L. Larger, IEEE J. Quantum Electron. **48**, 1415 (2012).
18. E. C. Levy, O. Okusaga, M. Horowitz, C. R. Menyuk, W. Zhou, and G. M. Carter, Opt. Express **18**, 21461 (2010).
19. L. Maleki, Nat. Photonics **5**, 728 (2011).
20. K. Saleh, R. Henriet, S. Diallo, G. Lin, R. Martinenghi, I. V. Balakireva, P. Salzenstein, A. Coillet, and Y. K. Chembo, Opt. Express **22**, 32158 (2014).
21. Y. C. Kouomou, P. Colet, N. Gastaud, and L. Larger, Phys. Rev. E **69**, 056226 (2004).
22. A. B. Cohen, B. Ravoori, T. E. Murphy, and R. Roy, Phys. Rev. Lett. **101**, 154102 (2008).
23. B. Ravoori, A. B. Cohen, J. Sun, A. E. Motter, T. E. Murphy, and R. Roy, Phys. Rev. Lett. **107**, 034102 (2011).
24. C. R. S. Williams, T. E. Murphy, R. Roy, F. Sorrentino, T. Dahms, and E. Scholl, Phys. Rev. Lett. **110**, 064104 (2013).
25. K. Ikeda, Opt. Commun. **30**, 257 (1979).
26. K. Ikeda, H. Daido, and O. Akimoto, Phys. Rev. Lett. **45**, 709 (1980).
27. K. Ikeda and M. Matsumoto, J. Stat. Phys. **44**, 955 (1986).
28. J.-P. Goedgebuer, P. Levy, L. Larger, C.-C. Chen, and W. T. Rhodes, IEEE J. Quantum Electron. **38**, 1178 (2002).
29. K. E. Callan, L. Illing, Z. Gao, D. J. Gauthier, and E. Scholl, Phys. Rev. Lett. **104**, 113901 (2010).
30. M. Nourine, Y. K. Chembo, and L. Larger, Opt. Lett. **36**, 2833 (2011).
31. Y. K. Chembo, L. Larger, R. Bendoula, and P. Colet, Opt. Express **16**, 9067 (2008).
32. L. Weicker, T. Erneux, O. D'Huys, J. Danckaert, M. Jacquot, Y. Chembo, and L. Larger, Phys. Rev. E **86**, 055201 (2012).
33. L. Weicker, T. Erneux, M. Jacquot, Y. Chembo, and L. Larger, Phys. Rev. E **85**, 026206 (2012).
34. L. Weicker, T. Erneux, O. D'Huys, J. Danckaert, M. Jacquot, Y. Chembo, and L. Larger, Philos. Trans. R. Soc. A **371**, 20120459 (2013).
35. J. H. T. Mbe, A. F. Talla, G. R. G. Chengui, A. Coillet, L. Larger, P. Woafo, and Y. K. Chembo, Phys. Rev. E **91**, 012902 (2015).
36. Y. K. Chembo, A. Hmima, P.-A. Lacourt, L. Larger, and J. M. Dudley, J. Lightwave Technol. **27**, 5160 (2009).
37. T. Erneux, *Applied Delay Differential Equations* (Springer, 2010).
38. M. Lakshamanan and D. V. Senthikumar, *Dynamics of Nonlinear Time Delay Systems* (Springer, 2011).
39. Y. C. Kouomou and P. Woafo, Phys. Lett. A **298**, 18 (2002).
40. Y. C. Kouomou and P. Woafo, Opt. Commun. **223**, 283 (2003).
41. Y. C. Kouomou and P. Woafo, Phys. Rev. E **67**, 046205 (2003).
42. A. M. Hagerstrom, T. E. Murphy, and R. Roy, Proc. Natl. Acad. Sci. USA **112**, 9258 (2015).